CDF/ANAL/HEAVY_FLAVOR/GROUP/1384
DRAFT VERSION 0.0

Measurement of the Efficiency of the Level 1 Central Muon Trigger at Low P_t

L. D. Gladney, J. B. González, R. E. Hughes, N. S. Lockyer

January 18, 1991

Abstract

The efficiency of the Level 1 Central Muon Trigger has been measured at low p_t with greater statistics than a previous study. A previously unused variable, the fit quality of the match between the muon stub and CTC track, is used to identify good muon candidates. We find the 50% efficiency value to be ~4.0 GeV/c for the *Central_Muon_5* triggers and ~ 2.0 GeV/c for the *Central_Muon_3*. These thresholds are lower than initially expected but are in agreement with an updated calculation. We find the average efficiency for muons with $p_t > 10$ GeV/c to be $0.976^{+0.015}_{-0.031}$ and $0.991^{+0.007}_{-0.021}$ respectively. We also conclude that the Δx cut applied by GMUFLT is too tight for low p_t muons. An alternative cut is proposed that is roughly independent of p_t.

I Introduction

The purpose of this study is to reduce uncertainties in the measured efficiency of the Level 1 Central Muon Trigger (Lv1CMT) at low p_t. The muon trigger efficiency bears importance to our measurement of the b-quark cross section that is being determined from the $B \rightarrow \Psi K$ sample. Uncertainties for this cross section due to the Lv1CMT previous measurement [1] were estimated to be at least 20%. Our analysis has reduced this error to < 5%.

In this note we briefly review the muon system hardware configuration and the principle of operation of the Lv1CMT. We then describe the procedure used to obtain the sample of level 1 unbiased muons from the muon data stream. The efficiency is then determined by taking the ratio of events with a level 1 hardware trigger bit set to the number of CMUO banks. We calculate the dependence of the efficiency on p_t and compare to the measured results. In the appendix we present in detail the calculation of the errors for the efficiency.

II Description of The Level 1 Central Muon Trigger

The central detector consists of 48 wedge shaped modules assembled in four self-supporting arches. Each wedge contains 4 layers of proportional drift cells for muon detection at the

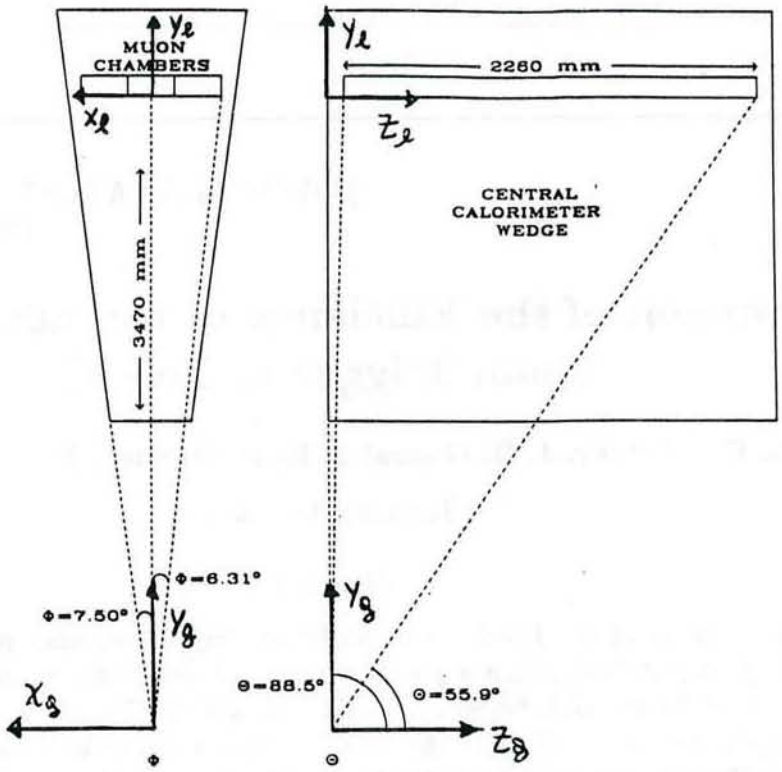

Figure 1: Location of the central muon chambers within a central calorimeter wedge. The coordinate systems shown are the *CDF global* and one of the *local* .

back of the hadron calorimeter section.[2] Each wedge is further subdivided in azimuth into 3 modules or chambers, roughly 4.2° each. Figure 1 shows the location of the muon chambers within a wedge. The chambers, shown in Figure 2, are composed of 16 cells arranged in four layers of 4 cells each. There are just 8 anode sense wires in a chamber because alternate cells in a layer share the same wire. A tower is made up of 8 cells arranged in two radial stacks separated by about 1.05° in ϕ. Four sense wires, one from each layer, make up a muon tower.

The Lv1CMT [3] requires that

$$Min(|t_4 - t_2|, |t_3 - t_1|) < t_{Max} \tag{2.1}$$

where $t_1, \ldots, t_4$ are the drift times to the sense wire for layers 1-4 and t_{Max} is a programmable threshold that can be varied in 1 ns steps. The effective cut on the angle α between the muon track candidate and the radial centerline is related to the difference in drift times by

$$\Delta t = H\frac{\alpha}{v_d} \tag{2.2}$$

valid for small α. The radial separation of sense wires between layers 1 and 3 (2 and 4) is $H = 0.0550$ m. The electron drift velocity, v_d, is about 50 μm/ns for a 50-50 argon-ethane gas with 1% ethanol admixture.

We next derive a simple expression for the p_t at which the efficiency of the level 1 trigger reaches the 50% point. We will compare to this expression later when discussing the final efficiency results. From the geometry shown in Figure 3 we can relate α to the p_t of a

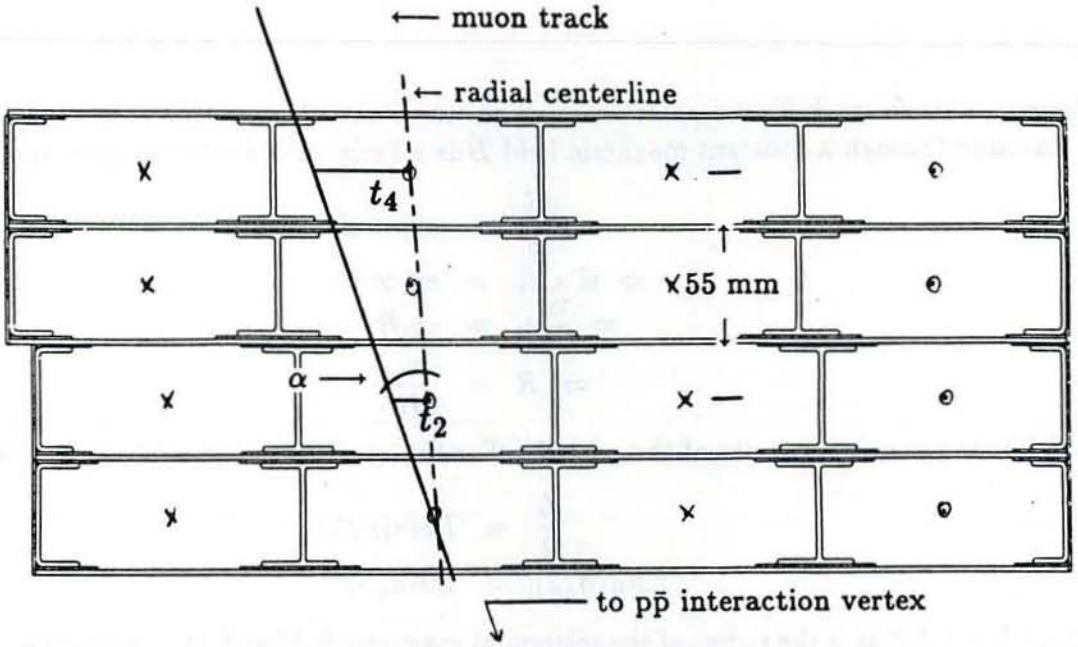

Figure 2: Cross section of a single muon chamber, showing drift times t_i, track angle α and anode wire. Notice that wires "x" and "o" in a same layer are connected at $\theta = 90°$.

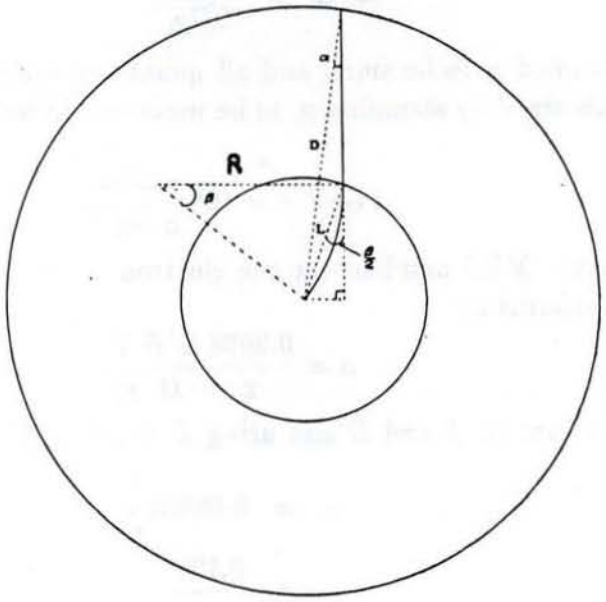

Figure 3: Transverse projection of a charged particle track. The inner circle of radius L is permeated by a magnetic field B. The radial distance of the closest anode wire to the center is given by D.

charged particle track from a $p\bar{p}$ collision. The trajectory of a relativistic particle of charge e traveling through a constant magnetic field $\vec{B}$ is a helix with radius R given by

$$\begin{aligned} \frac{d\vec{p_t}}{dt} &= e\vec{v_t} \times \vec{B} \\ \Rightarrow \vec{\omega} \times \vec{p_t} &= e\vec{v_t} \times \vec{B} \\ \Rightarrow \frac{v_t}{R} p_t &= e v_t B \\ \Rightarrow R &= \frac{p_t}{eB} \end{aligned} \tag{2.3}$$

and $\vec{\omega}$ is the angular velocity of the particle. For the quantities defined in Figure 3 we have

$$\frac{L}{2} = R sin(\beta/2) \tag{2.4}$$

$$L sin(\beta/2) = D sin(\alpha) \tag{2.5}$$

where $L = 1.440$ m is the radius of the solenoidal magnetic field and $D = 3.470$ m is the radial distance from the interaction point to the innermost muon chamber anode wire. Combining equations (2.3), (2.4) and (2.5) we get

$$\begin{aligned} \frac{L}{2} &= \frac{p_t}{eB} \frac{D}{L} sin(\alpha) \\ \Rightarrow \alpha &= \frac{eL^2 B}{2Dp_t} \end{aligned} \tag{2.6}$$

where we have assumed α to be small and all quantities are in the MKS system. A more useful relation is obtained by assuming p_t to be measured in units of GeV/c. The conversion factor is given by

$$1\, GeV/c = 10^9 \frac{e}{c} \frac{Joule}{m/s} \tag{2.7}$$

where e and c are the MKS numbers for the electron charge and the speed of light. Then equation (2.6) transforms to

$$\alpha = \frac{0.2998}{2} \frac{L^2 B}{D} \frac{1}{p_t}. \tag{2.8}$$

Replacing the values for L and D and using $B = 1.4116$ T we get

$$\alpha = 0.08958 \frac{B}{p_t} \tag{2.9}$$

$$= \frac{0.126}{p_t} \tag{2.10}$$

where α and p_t are measured in radians and GeV/c respectively. Equations (2.2) and (2.9) allow us to relate t_{Max} to a critical transverse momentum $P_{50\%}$ given by

$$P_{50\%} = 0.08958 \frac{BH}{v_d} \frac{1}{t_{Max}} \tag{2.11}$$

III Selection of Events

Identification of a large sample of real muons is necessary in order to map the efficiency of the muon trigger at low p_t. The muon stream was used as our source of unbiased muon events. We found roughly 10 times more unbiased muon events at low p_T using the muon stream than A. Gauthier found using the electron stream (to use the muon stream was suggested by Alain).

III.1 Unbiased Data

The events kept on files Muo04 have passed the muon production filter GMUFLT. The filter GMUFLT selects events based on CMUO and FMUO bank information. When the event contains at least one FMUO bank, GMUFLT keeps the event automatically.[4] If the event contains no FMUO bank, then at least one muon candidate (a CMUO bank) is required to satisfy

$$|\Delta x| < 10.0\ cm \tag{3.12}$$

$$p_t > P_c \tag{3.13}$$

The variable Δx represents the difference in the x intercepts of the CTC track and the muon stub (see next subsection). This cut rejects events that undergo large multiple scattering and in general increases the probability that the track is a real muon. It is felt that this cut does not contain bias in favor of events triggering on muons. Equation (3.13) reduces the statistics of low momentum bins but does not introduce bias. The value of P_c depends on what triggered the event and is described in reference [4].

It was necessary to keep only the CMUO, CMUS, and TCMD [5] banks listed in Table 1 for this analysis. We selected our data sample, using the module TRVIEW, and also requiring each passing event to have at least one CMUO bank.

Bank name	*Description*
CMUO	Central muon object bank
CMUS	Muon stub information
TCMD	Trigger central muon matchbox detector bank

Table 1: Banks kept for our analysis.

We selected the events from the muon stream that triggered by at least one non-muon trigger in order to obtain the unbiased data. The list of triggers [6] we accepted are shown

Trigger name	*Level*
Missing*	3
Jet*	3
Trijet*	3
Total*	3
Electron_central*	3
Photon*	3
Diphoton*	3
Dielectron*	2
Electron_plug*	3
Forward*	3

Table 2: Events had to satisfy one of the above triggers.

Table 2. From reference [6], section II, an event that passes any of these triggers was written to tape. We kept roughly 7.7% of the events for 5 GeV/c and about 14% for the 3 GeV/c study respectively, after the above conditions were satisfied.

III.2 Muon Isolation

The event sample obtained with the procedure of the previous section contains a large number of muon candidates that are not real muons. In order to reduce the number of fake muons we apply a new cut to the muon candidates based on the fit quality of the match between the CTC track and the muon stub, which we call Q^2. It is better to use a cut that is roughly independent of muon p_t, such as Q^2, rather than the Δx cut of GMUFLT. In order to further motivate this cut, we discuss briefly its definition, the sources of fake muons and then present results.

The production module CMLNK links the CTC track and the muon stub and returns a fit quality. In more detail, CMLNK applies the following procedure to create one of these banks.

1. Extrapolate each central track to the central muon detector and express final trajectory in local wedge coordinates.

2. For each muon stub find all central tracks extrapolating to the tower containing the stub.

3. Choose the track that minimizes the covariance form Q^2 for the match.

In a cartesian coordinate system a straight line can always be described as

$$\begin{aligned} x_l &= \alpha_x y_l + x_0 \\ z_l &= \alpha_z y_l + z_0 \end{aligned} \tag{3.14}$$

with

(x_l, y_l, z_l) : local wedge coordinates of straight line.

α_x, α_z : slopes for the projections of original straight line on planes (x-y) and (z-y) respectively.

x_0, z_0 : x and z intercepts for these projections.

The stub and the track projection are straight lines and we can measure their difference as

$$\begin{aligned} \Delta\alpha &\equiv \alpha_x^{track} - \alpha_x^{stub} \\ \Delta x &\equiv x_0^{track} - x_0^{stub}. \end{aligned} \tag{3.15}$$

The corresponding quantities for the (z-y) projection are not used because of poor quality of their measurement. Q^2 is calculated as

$$Q^2 = \Delta\alpha V_{\alpha\alpha}^{-1}\Delta\alpha + 2\Delta\alpha V_{\alpha x}^{-1}\Delta x + \Delta x V_{xx}^{-1}\Delta x \tag{3.16}$$

with V the estimated covariance matrix for the variables $(\Delta\alpha, \Delta x)$. Because $\Delta\alpha$ and Δx are correlated [9] we do not know how to predict the distribution of Q^2. If $\Delta\alpha$ and Δx were independent variables, the Q^2 parent distribution would be a χ^2 distribution with two degrees of freedom ($\nu = 2$). Figure 4 shows the distribution of Q^2 for CMUO banks from the J/Ψ dimuon sample. We also plot the distribution of probability for $\nu = 1, 2, 3$. We see the Q^2 distribution behaves like a χ^2 distribution with $\nu = 2$.

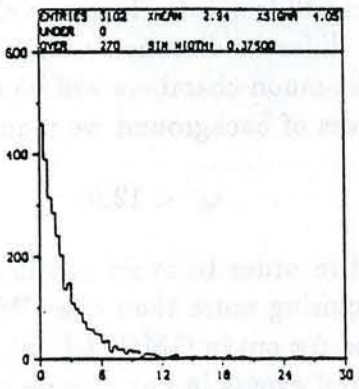

Figure 4: Measured distribution of Q^2 using muons from J/ψ decay.

It is rare to have real muons (not strongly interacting) as immediate products of $p\bar{p}$ collisions. Produced particles are mainly pions, kaons and protons. A list of sources of fake muons is [10]

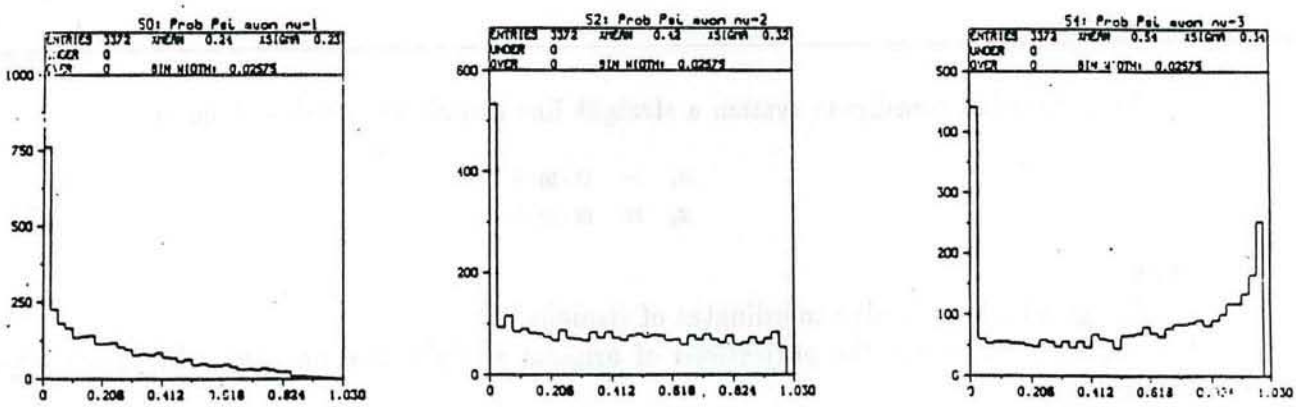

Figure 5: χ^2 probability distribution for muons from J/ψ decay for $\nu = 1, 2, 3$ degrees of freedom.

1. Non interactive punchthrough.

2. Meson decay in flight.

3. Interactive punch through (shower leakage).

Hadrons that do not interact in the calorimeter cannot be distinguished from real muons. For the purpose of this study they are as useful as real muons and we do not remove them.

The muon from the decay of a pion or kaon will have a different direction than the parent particle. This can cause tracks with true $p_t = P_{True}$ to be measured by the CTC as having lower or higher p_t. Therefore decays in flight can be a source of incorrectly measured p_t tracks. These tracks can thus be incorrectly entered in the efficiency versus p_t plots.

Hadrons that interact in the steel of the wedges generate a shower of particles. Sometimes one or a few secondary particles will leak into the muon chambers producing a "muon" stub. Because the muon candidates differ in direction with respect to the incoming hadron we have that the apparent p_t at the muon chambers will be different respect to the CTC value.

To diminish these two sources of background we request

$$Q^2 < 12.0. \tag{3.17}$$

A loose Q^2 cut was applied in order to avoid possible bias from the $\Delta\alpha$ dependence of Q^2. We test the Q^2 cut by requiring more than one CMUO bank per event. This reduces the effect of equation (3.12), the Δx cut in GMUFLT, which is applied to only one muon per event. Roughly 45% of the muon events in our sample are multi-muon events. The effects of the Q^2 cut can be seen in Figures 8 through 11. Obvious improvement in signal to noise is seen in the hadronic energy deposited plot and the Δx plot. The truncated appearance of Figure 11 around 10 cm is caused by the GMUFLT cut. The large tail is evidence for the extra muons per event to which the Δx cut was not applied.

We now apply in addition to the Q^2 cut the following isolation cuts:

$$0.05 < E(EM) < 1.0\ GeV$$
$$0.50 < E(Had) < 3.5\ GeV \qquad (3.18)$$

The symbols $E(EM)$ and $E(HAD)$ refer to the energy deposited in the electromagnetic and hadronic calorimeter tower by the muon candidate. The values chosen for the isolation cuts are motivated by a study of muons from J/ψ decay, the results of which are shown in Figures 6 and 7.

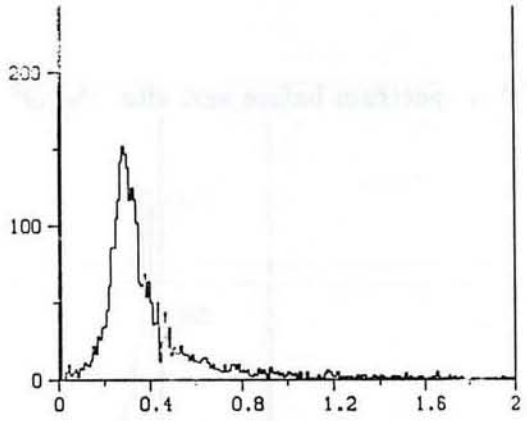

Figure 6: Measured electromagnetic energy deposition distribution from muons in J/ψ decay.

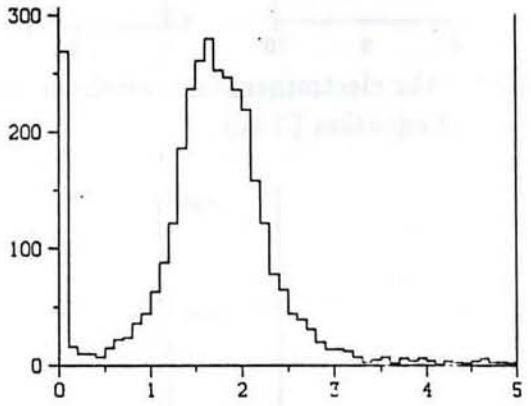

Figure 7: Measured hadronic energy deposition distribution from muons in J/ψ decay.

Figures 12 through 15 show the effects of requirements from equations (3.17 and 3.18). It is evident from Figure 12, energy deposition in the hadron calorimeter, that the Q^2 and energy isolation cuts provide a clean real muon sample. The data for this study uses the full unbiased muon sample and therefore includes events with one CMUO bank.

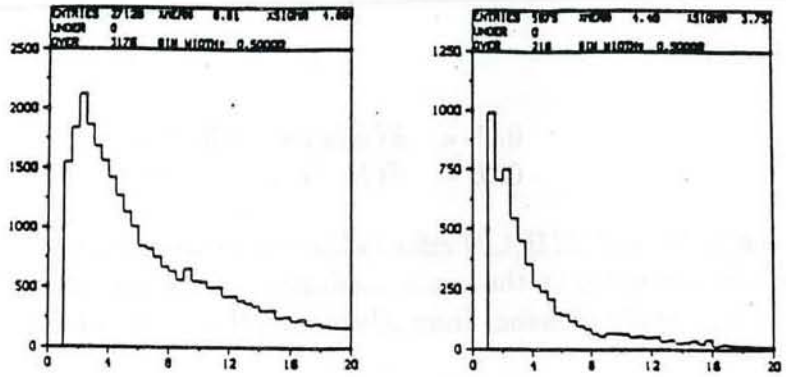

Figure 8: CMUO p_t spectrum before and after the Q^2 cut of equation (3.17).

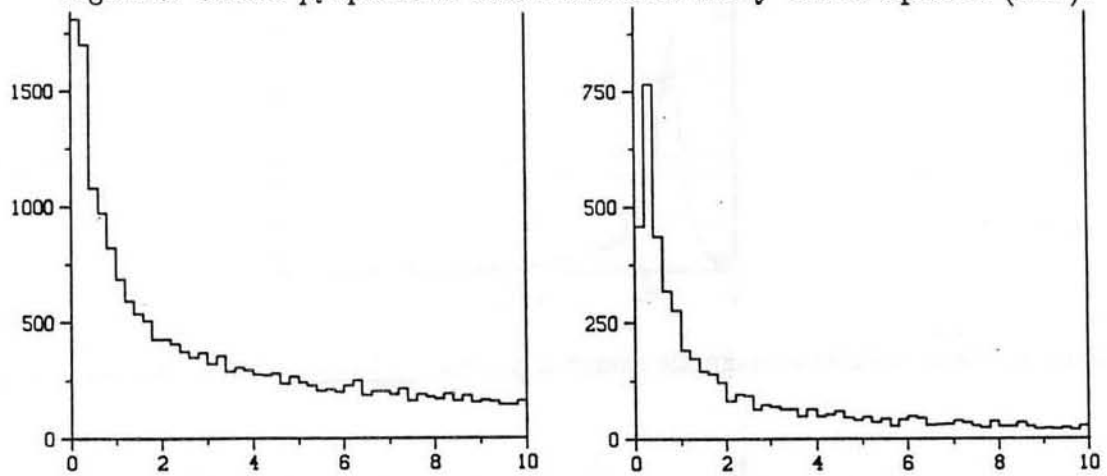

Figure 9: Energy deposited in the electromagnetic calorimeter in the tower around the muon before and after the Q^2 cut of equation (3.17).

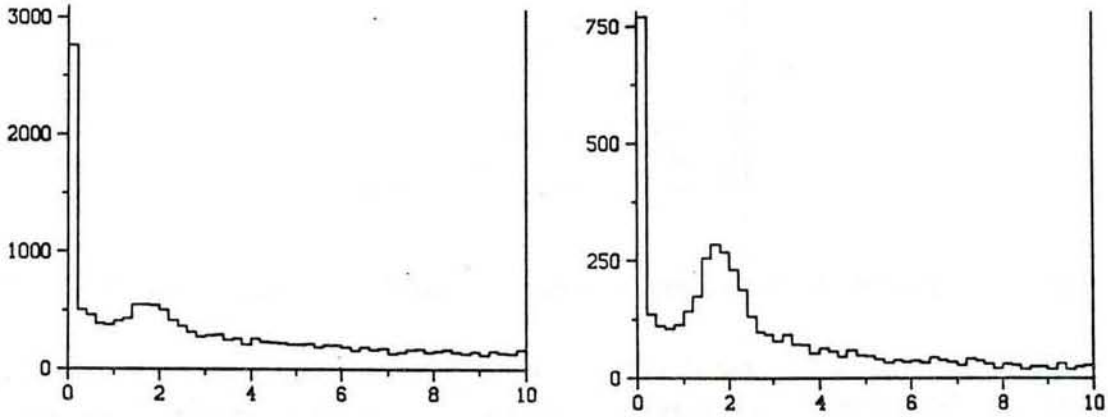

Figure 10: Energy deposited in the hadron calorimeter in the tower around the muon before and after the Q^2 cut of equation (3.17).

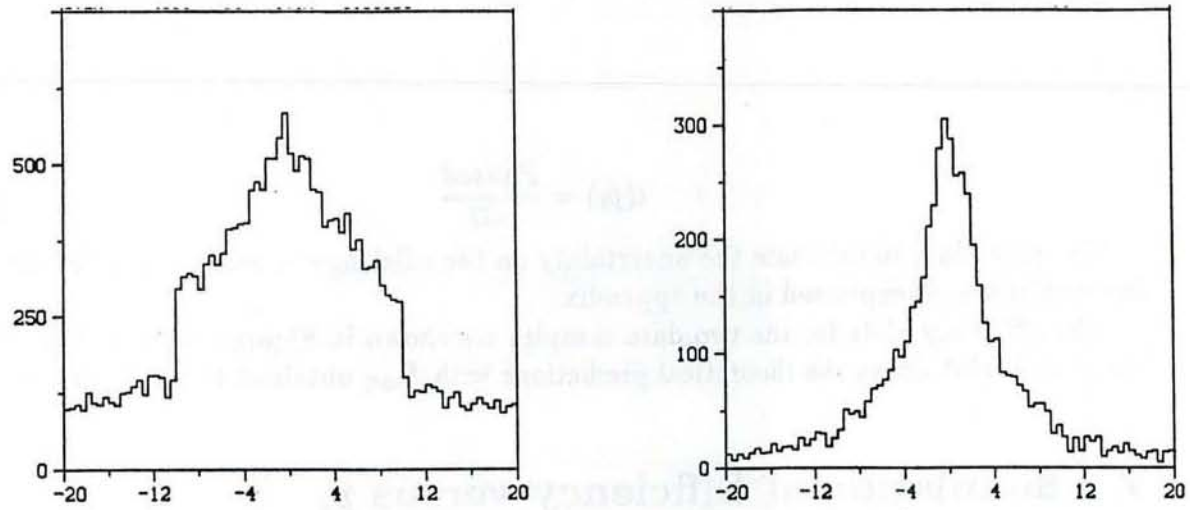

Figure 11: Distribution of Δx, equation (3.15), before and after the Q^2 cut. The effect of the $\Delta x < 10$ cm cut, equation (3.12), can be seen even though we required more than one CMUO per event.

IV Analysis Procedure

The CMUO banks contain the results of the matching between central muon stubs and CTC tracks. This bank contains the initial p_t of the track and a pointer to the CMUS bank containing the location of the muon tower. The TCMD bank contains the Lv1CMT bit status. The information is unpacked from 24 registers whose first 16 bits are described in Table 3.

Bits	*Contents*
00-05	Lv1CMT status for West side
06	'OR' of six previous bits
07	WGold
08-13	Lv1CMT status for East side
14	'OR' of six previous bits
15	EGold

Table 3: Organization of Lv1CMT bit status in 1 of 24 TCMD registers.

We unpack TCMD with the Fortran instruction BTest. We note the numbering of the towers inside a wedge (0:5) is reversed in TCMD with respect to CMUS for the East arches. So tower 5 in TCMD corresponds to tower 0 in CMUS. This is not the case for the West arches where tower 5 in TCMD corresponds to tower 5 in CMUS.

For each CMUO bank we fill a histogram entitled *All.* The corresponding tower bit in the TCMD word is checked and if true a histogram entitled *Passed* is filled. The efficiency is calculated as the ratio

$$\epsilon(p_t) = \frac{Passed}{All} \tag{4.19}$$

The procedure to calculate the uncertainty on the efficiency or more correctly, the confidence intervals, is explained in the appendix.

The efficiency plots for the two data samples are shown in Figures 16 and 17. The solid line in each plot shows the theoretical predictions with $P_{50\%}$ obtained from equation (2.11).

V Simulation of Efficiency versus p_t

Without the effect of multiple scattering included, the efficiency of the Lv1CMT plotted versus p_t is a step function with transition at $P_{50\%}$. Multiple scattering smooths this transition because a particle with initial momentum p_t could have any final angle α. Therefore the equation (2.9) should be interpreted as the average value of α. It is straighforward to compute the shape of the transition due to multiple scattering. Curves for five possible thresholds are shown in reference [1].

VI Results and Conclusions

The Level 1 Muon trigger efficiency plots for the two data samples are shown in Figures 16 and 17. The Q^2 and energy isolation cuts, equations (3.17) and (3.18), have been applied to these figures. We find the $P_{50\%}$ efficiency point to be $\sim$ 4.0 GeV/c and $\sim$ 2.0 GeV/c for the $Central\_Muon\_5$ and $Central\_Muon\_3$ triggers respectively. We have reduced the uncertainty in the measured efficiency by about a factor of 5 by using the muon stream as the source of unbiased events. The shape near threshold is smoothly varying, unlike the earlier study [1] which had low statistics in this p_t region. The solid line in each plot shows the theoretical predictions with $P_{50\%}$ obtained from equation (2.11). We used $B = 1.4116$ T and $v_d = 50.0\ \ \mu m/ns$. This gives the calculated $P_{50\%}$ of 4.6 GeV/c and 2.0 Gev/c, in agreement with the measured values.

We also conclude that the Δx cut of 10 cm, used by the production filter GMUFLT, is inefficient for low p_t and is ineffective for high p_t. We have proposed to eliminate the Δx cut in favor of the Q^2 cut.

References

[1] Alain Gauthier, *Efficiency of the Level 1 Central Muon Trigger*, CDF Note 937 (August, 1990).

[2] G. Ascoli et al., *CDF Central Muon Detector* NIM A268 (1988) 33-40 (also CDF NIM p.218).

[3] G. Ascoli et al., *CDF Central Muon Level 1 Trigger Electronics*, NIM A267 (1988) 63-67 (also CDF NIM p.272).

[4] Tony Liss, *GMUFLT: The Muon Filter in Production*, CDF Note 1080.

[5] Craig Blocker et al., *The CDF Event Structure vs. 3.12*, CDF Note 152 (June, 1990). An online copy can be found as CDF$Root4:[Documents] CDF152.Mem .

[6] Jay Hauser, *Guide to The Triggers Used in the 1988-1989 CDF Data Run*, CDF Note 966, (June, 1989).

[7] W. T. Eadie et al., *Statistical Methods in Experimental Physics*, North-Holland (1971).

[8] Lee Holloway, private communication.

[9] Particle Data Group, *Review of Particles Properties*, Physics letters B. 239 (1990).

[10] David A. Smith, *Study of Muons Associated with Jets in Proton AntiProton Collisions at* $\sqrt{s} = 1.8$ *TeV*, Thesis, University of Illinois (1989).

A Confidence Intervals for the Binomial Distribution

We present in detail the method used to calculate confidence intervals for the efficiency. [7] For a given p_t, the probability that n muons pass condition (1) out of N total attempts is given by

$$P(n) = \binom{N}{n} p^n (1-p)^{N-n} \qquad n = 0, 1, \ldots, N \tag{1.20}$$

with p the probability of 1 muon being detected out of 1 attempt. If p is unknown, an unbiased estimate of the variance is given by

$$V(n) = \left(\frac{N}{N-1}\right) N \left(\frac{n}{N}\right)\left(1 - \frac{n}{N}\right) \tag{1.21}$$

Equation (1.21) is the correct way of calculating uncertainties for the bin counts of a histogram for large N. This formula has two problems for our application. One is the fact that it predicts symmetric intervals and the other is that for $n = 0$ or N, it gives $V(n) = 0$, which is clearly wrong. This is relevant for an efficiency error calculation because n is 0 or N for most p_t's. The correct way of establishing a confidence interval for p is by solving

$$\frac{1-\beta}{2} = \sum_{r=0}^{n} \binom{N}{r} p_h^r (1-p_h)^{N-r} = \sum_{r=n}^{N} \binom{N}{r} p_l^r (1-p_l)^{N-r} \tag{1.22}$$

where p_l, p_h define the limits of the confidence interval around $\epsilon = n/N$ with probability β. After a small rearrangement we transform this equation to

$$\begin{aligned} \sum_{r=0}^{n} \binom{N}{r} p_h^r (1-p_h)^{N-r} &= \frac{1-\beta}{2} \\ \sum_{r=0}^{n-1} \binom{N}{r} p_l^r (1-p_l)^{N-r} &= \frac{1+\beta}{2} \end{aligned} \tag{1.23}$$

The solution to eq. (1.23) can be found with a binary search. [8] To prove the uniqueness of the solution one needs to verify that the left hand side of eq. (1.23) is a monotonically decreasing function of p for $0 < p < 1$.

Proof

Define

$$f(p) = \sum_{r=0}^{n} \binom{N}{r} p^r (1-p)^{N-r} \tag{1.24}$$

By using the normalisation condition we get

$$f(p) = 1 - \sum_{r=n+1}^{N} \binom{N}{r} p^r (1-p)^{N-r} \tag{1.25}$$

Taking derivatives

$$\begin{aligned}\frac{df}{dp} &= \sum_{r=0}^{n}\binom{N}{r}p^{r-1}(1-p)^{N-r-1}(r-Np) \\ &= -\sum_{r=n+1}^{N}\binom{N}{r}p^{r-1}(1-p)^{N-r-1}(r-Np) \qquad (1.26)\end{aligned}$$

The first expression is clearly negative for $p > n/N$ while the second is clear for $p < (n+1)/N$. QED.

In tables 4 through 6 we give values obtained from the numerical solution of (1.23) with $\beta = 0.683$ and for comparison we tabulate values obtained with

$$\sigma_1 = \sqrt{\frac{1}{N-1}(\frac{n}{N})(1-\frac{n}{N})} \qquad (1.27)$$

$$\sigma_2 = \frac{\sqrt{n(1+\frac{n}{N})}}{N}. \qquad (1.28)$$

The first expression comes from eq. (1.21) by taking the root square and dividing by N. The second one is the naive propagation of errors through a ratio with n and N treated as independent variables.

r	ϵ	$\epsilon - p_l$	$p_h - \epsilon$	σ_1	σ_2
0	0	0	0.31	0	0
1	0.2	0.17	0.32	0.20	0.21
2	0.4	0.25	0.30	0.24	0.33
3	0.6	0.30	0.25	0.24	0.44
4	0.8	0.32	0.17	0.20	0.53
5	1.0	0.31	0	0	0.63

Table 4: Comparison for N=5, $\beta = 0.683$.

r	ϵ	$\epsilon - p_l$	$p_h - \epsilon$	σ_1	σ_2
0	0	0	0.17	0	0
2	0.2	0.13	0.21	0.13	0.16
5	0.5	0.20	0.20	0.17	0.27
8	0.8	0.21	0.13	0.13	0.38
10	1.0	0.17	0	0	0.45

Table 5: Comparison for N=10, $\beta = 0.683$.

r	ϵ	$\epsilon - p_l$	$p_h - \epsilon$	σ_1	σ_2
0	0	0	0.018	0	0
20	0.2	0.042	0.048	0.040	0.049
50	0.5	0.055	0.055	0.050	0.087
80	0.8	0.048	0.042	0.040	0.120
100	1.0	0.018	0	0	0.141

Table 6: Comparison for N=100, $\beta = 0.683$.

B Figures

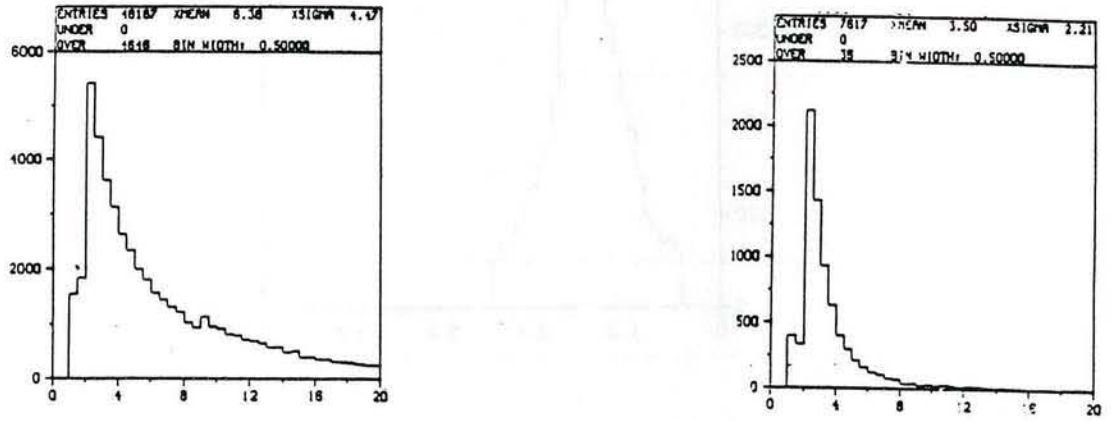

Figure 12: Muon candidates p_t spectrum before and after the combined Q^2 and energy isolation cuts.

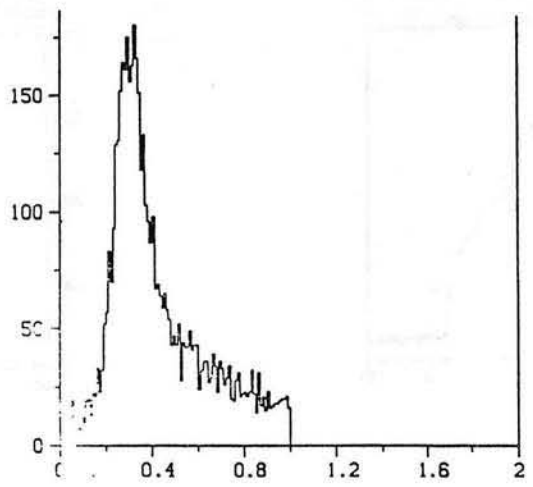

Figure 13: Energy deposited in the electromagnetic calorimeter in the tower around the muon, before and after the Q^2 and energy isolation cuts.

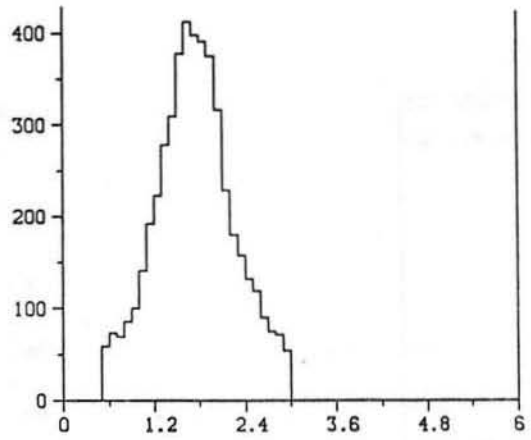

Figure 14: Energy deposited in the hadron calorimeter in the tower around the muon, before and after the Q^2 and energy isolation cuts.

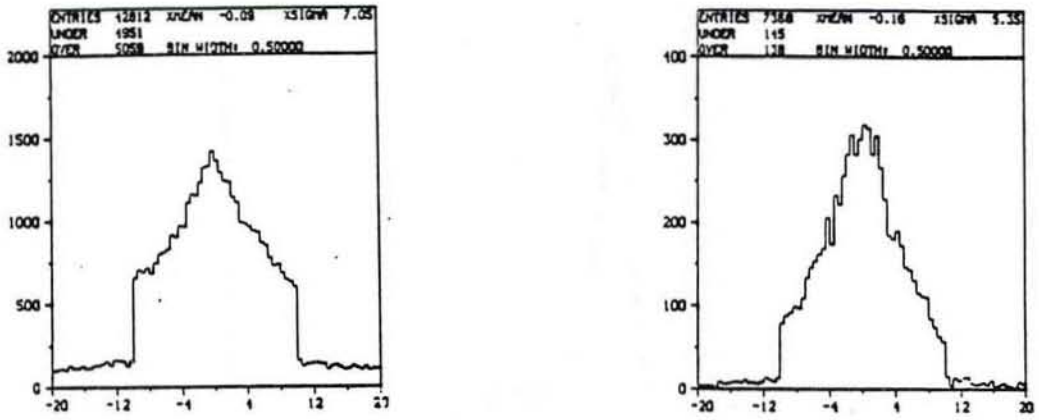

Figure 15: Distribution of Δx, equation (3.15), before and after the Q^2 and energy isolation cuts. The effect of the $\Delta x < 10$ cm cut, equation (3.12), can be seen.

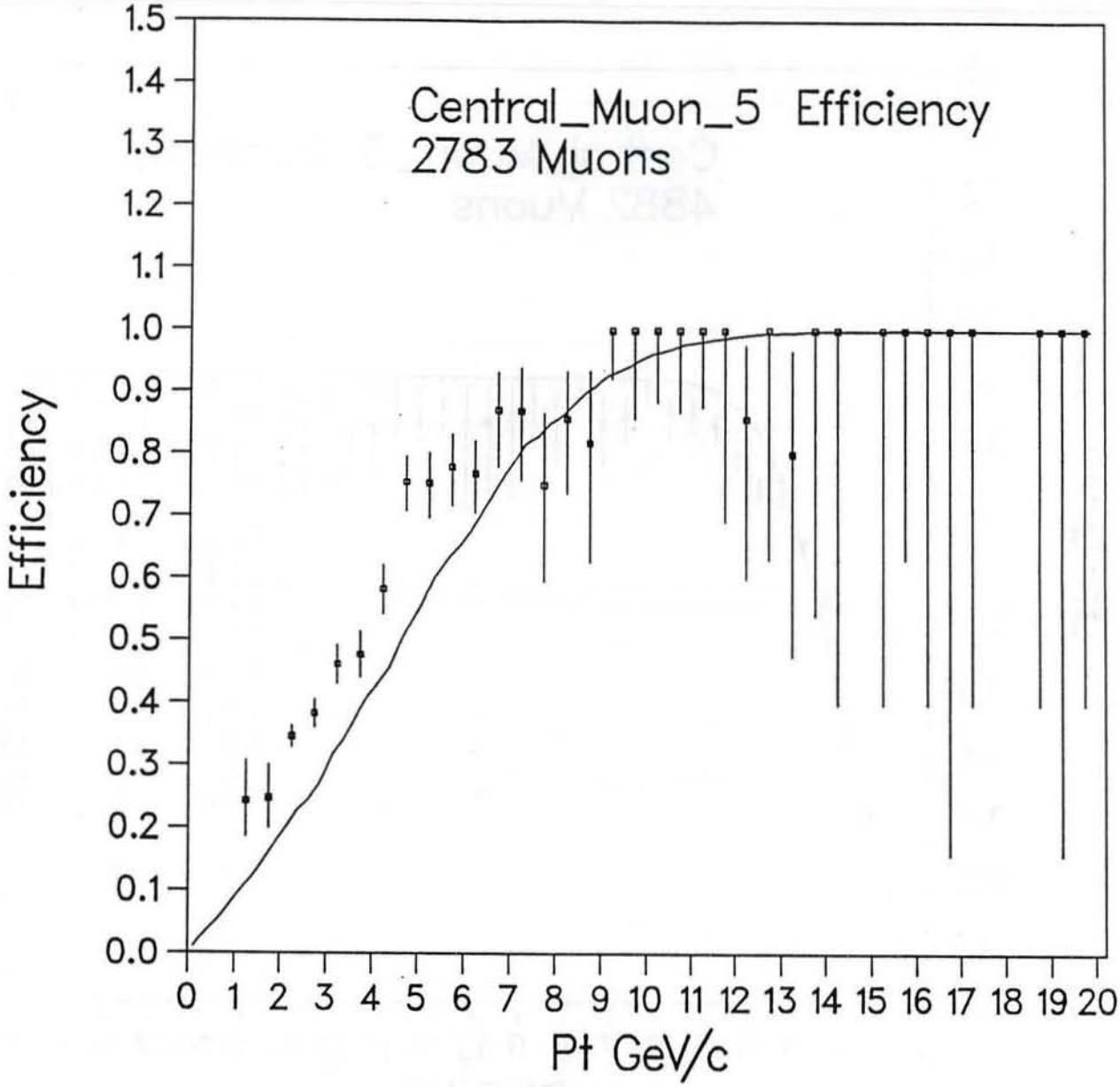

Figure 16: Efficiency for 5 GeV/c trigger. Error bars are for a 68% confidence level.

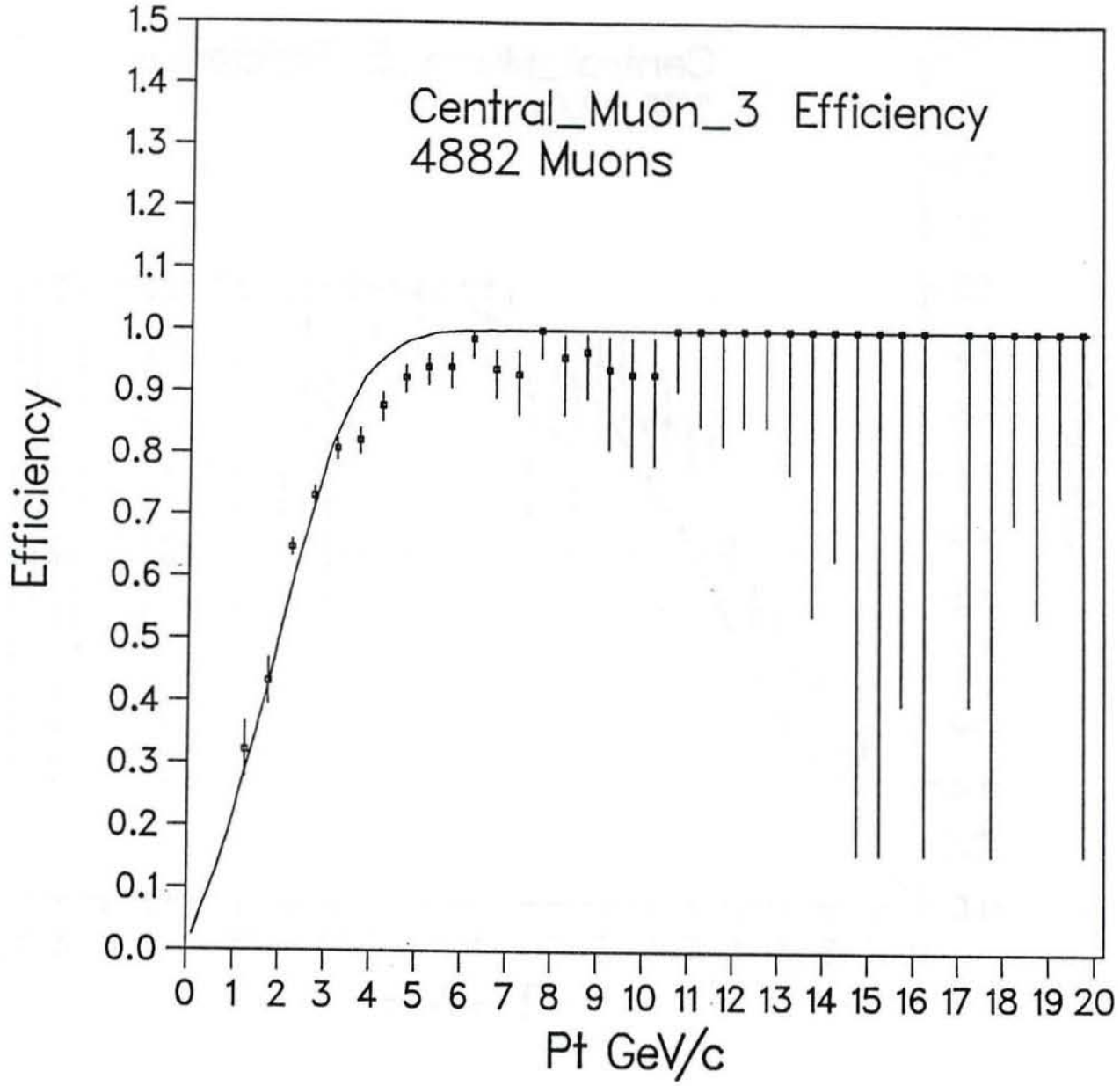

Figure 17: Efficiency for 3 GeV/c trigger. Error bars are for a 68% confidence level.

C Comments

As it was explained in subsection III.1, we required that at least one of the triggers displayed in table 2 was satisfied. This scheme to avoid bias works if we can prove that there is no correlation between Central_Muon_3 and any of those triggers. From the definition for the triggers it is not clear that this is not the case. Some of the triggers require a level 1 of the same type but others do not. None of them explicitely requires a level 1 Central_Muon trigger, so the correlation, if there is one, should not be high.

To check our data we analysed the trigger status for 200 events (after cuts) from the Central_Muon_3 data. The level 1 triggers they came through are shown in table 7. In table 8 we show the level 2 triggers they satisfied. From these tables no correlation can be seen.

trigger name	percentage
Jet_1_18	99.5
Central_electron_3_3	90.5
Photon_4_6_V2	92.4
Central_Electron_6_6_V2	81.2

Table 7: Level 1 triggers for Central_Muon_3 data.

trigger name	percentage
Total_Et_120	33
Electron_EMC_12_6_Prereq_V3	34
Missing_Et_25_Tex_8_Not_Fwd	33
Electron_Emc_5_CMu_3	24

Table 8: Level 2 triggers for Central_Muon_3 data.

Consultations about this work can be done to UPENN1::Julio.